Optically Sensorized Elastomer Air Chamber for Proprioceptive Sensing of Soft Pneumatic Actuators

Jaewoong Jung, Myungsun Park, DongWook Kim, and Yong-Lae Park

***Abstract*—Soft robotics has proven the capability of robots interacting with their environments including humans by taking advantage of the property of high compliance in recent years. Soft pneumatic actuators are one of the most commonly used actuation systems in soft robotics. However, control of a highly compliant actuation system remains as a challenging issue due to its nonlinearity and hysteresis. Addressing this problem requires integration of a soft sensing mechanism with the actuator for proprioceptive feedback. A soft optical waveguide with a reflective metal coating is a promising sensing mechanism with high compliance and low hysteresis. In this letter, we propose design and fabrication of a soft pneumatic actuator integrated with an optical waveguide that can provide the proprioceptive information of the actuator. We describe the design and fabrication, and present experimental characterization results of the proposed system. We also provide applications of the proposed system.**

***Index Terms*—Hydraulic/pneumatic actuators, soft sensors and actuators, soft robot materials and design.**

I. Introduction

ROBOTIC systems, which have been designed to substitute human labors in industry fields, are becoming more versatile recently and subsequently expanding their application areas even to our everyday lives. Safety in human-robot interaction (HRI) is more emphasized these days for this reason, and physical compliance in design can be an immediate solution to increasing the safety [1], [2]. This can be achieved by soft robotics technologies that can significantly enhance the adaptability of robots to environments compared to conventional robots consisting of rigid linkages and descrete joints [3], [4].

Actuation in soft robots can be achieved by various mechanisms, such as pneumatic artificial muscles [5]–[7], tendon-driven systems [8], [9], shape memory materials [10], [11], and electroactive polymers [12], [13]. Among these methods, a pneumatic muscle achieved by inflation of a soft elastomer chamber is widely used due to the easiness in design variations for different actuation modes, such as contraction, extension, and bending [14], as well as its low-cost and simple fabrication process [15]. However, there always exists a challenge of control in this type of systems due to the complexity in modeling of the actuation dynamics and the inherent hysteresis of the host polymer structures. To address this issue, sensorized actuators have been proposed for proprioceptive feedback by directly embedding (or integrating) soft sensors in the actuator bodies [16]–[18]. The soft sensors to be integrated with soft actuators should be not only compact but also highly stretchable so that they do not degrade the performance of the host actuators. There have been different approaches to build soft sensors, such as microfluidic channels embedded in elastomer structures [19], [20], conductive fabrics [21], [22], dielectric polymer layers [23], [24], and stretchable optical waveguides [17], [25]–[27]. Among these mechanisms, microfluidic sensors and optical waveguides, both having high compliance, are widely used in system integration. Microfluidic soft sensors measure the change of electrical resistance of the embedded microchannels filled with conductive liquid, caused by deformation of the channels when mechanical stresses are applied [19]. In spite of their simplicity in mechanism and fabrication, there is always a possibility of leakage of the liquid. However, soft optical sensors, which detect optical power loss in a stretchable waveguide caused by mechanical deformation [25], are free from the leakage issue and thus have a higher potential in practical applications.

Therefore, we focus on optical soft sensors for integration with soft actuators in this study. One of the key criteria of a soft sensor to be embedded in a soft actuator is that it should not degrade the performance of the actuator. In other words, addition of a soft sensor should not change the actuation properties of the host system, such as compliance and dynamics.

In this letter, we propose a pneumatic bending actuator that directly uses the air chamber for actuation as a soft optical waveguide for proprioceptive feedback. Soft bending actuators, have been widely used for different tasks, such as grasping, manipulation, and locomotion. However, due to the inherent structural characteristics of the bending actuators, it is challenging to embed a sensor for estimating its state while not disturbing the dynamics of the actuator. We propose to solve this problem by integrating a soft optical waveguide in the actuator.

Fig. 1(a) shows the light propagating through the proposed waveguide. Fig. 1(b) shows the pneumatic actuator with two elastomeric layers of different stiffnesses, bending when the

Manuscript received September 10, 2019; accepted January 12, 2020. Date of publication February 3, 2020; date of current version February 19, 2020. This letter was recommended for publication by Associate Editor G. Endo and Editor P. Rocco upon evaluation of the reviewers' comments. This work was supported in part by NAVER LABS Corporation and in part by the National Research Foundation of Korea funded by the Korean Government (MSIT) under Grant NRF-2016R1A5A1938472. *(J. Jung and M. Park contributed equally to this work.) (Corresponding author: Y.-L. Park.)*

The authors are with the Department of Mechanical Engineering, the Institute of Advanced Machines and Design (IAMD), the Institute of Engineering Research, Seoul National University, Seoul 08826, South Korea (e-mail: 7jaewoong7@snu.ac.kr; arielrbts@snu.ac.kr; shigumchis@snu.ac.kr; ylpark@snu.ac.kr).

This letter has supplementary downloadable material available at https://ieeexplore.ieee.org, provided by the authors.

Digital Object Identifier 10.1109/LRA.2020.2970984

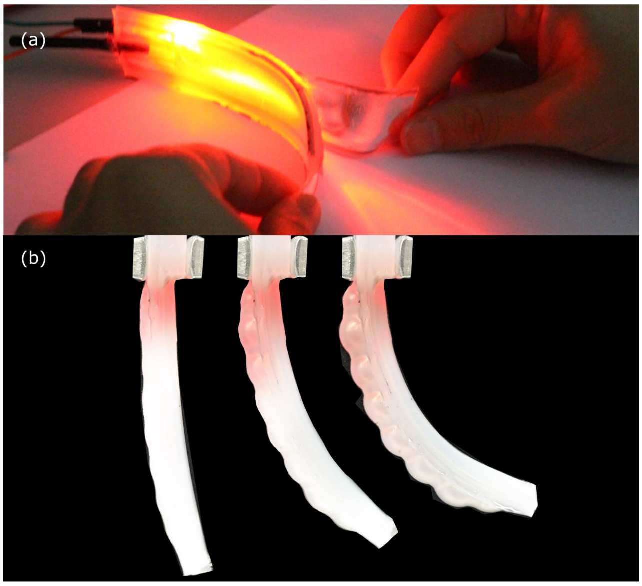

Fig. 1. (a) Propagation of light through air chamber surrounded by elastomer layer coated with reflective silver layer. (b) A prototype of a pneumatic actuator with air channel coated with reflective layer. The layer on the right side is thinner than the other one, which generates more microcracks. Since the light emitted from an LED on the top is transmitted throughout the channel, the stretched elastomeric layer with microcracks shows red light.

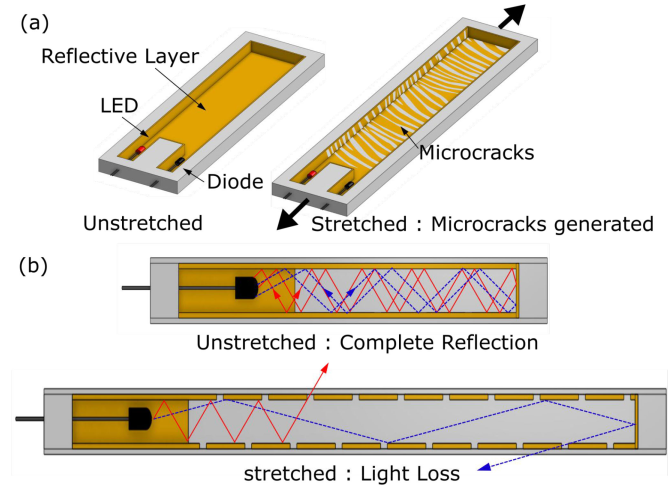

Fig. 2. Schematic of the optical sensing mechanism. When the waveguide is deformed, microcracks form on the undeformable metal layer, letting the light to escape. As a result, light intensity measured by the photodiode drops.

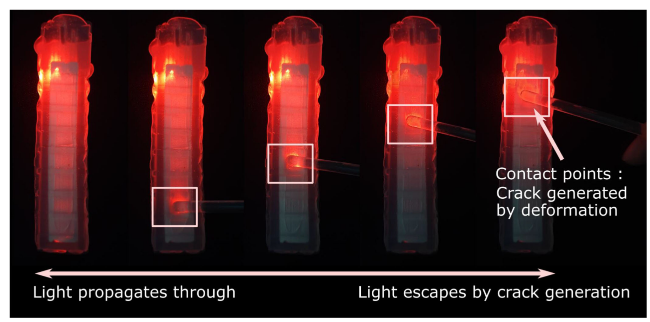

Fig. 3. The propagation of light through the waveguide under external contact. Microcracks are generated on the point of the contact, letting the light to escape. It can be seen that the light could not propagate beyond the point of the contact, since it had escaped through the generated microcracks.

chamber is pressurized with compressed air. The air chamber contains a light-emitting-diode (LED) and a photodiode, and the inside wall of the chamber is coated by a thin metallic reflective layer for light propagation. When pressurized, only the softer layer is stretched, generating bending motions. During this process, the strain in the chamber wall causes microcracks on the thin rigid metallic layer, resulting in optical power loss of the light from the LED through the chamber wall. The main advantage of the proposed design is that the actuator can maintain its original compact form factor as well as the functionality even with the integration of the sensor. In addition to the design, we propose a new manufacturing method that enables uniform and robust coating of a thin metal layer on a polymer surface, which has not been easy with conventional deposition processes. The coated layer showed strong bonding to the polymer surface and did not degrade over repeated deformation.

II. Soft Optical Waveguide

A. Design

Optical soft sensors have a simple sensing mechanism that uses the change in light intensity with mechanical deformation. An LED and a photodiode are embedded in the soft elastomeric waveguide, so that the light emitted from the LED propagates through the waveguide to the photodiode by internal reflection. The waveguide transmits the light from the LED in the initial state. However, if it is deformed (e.g. bent or stretched), part of the light escapes through the wall of the waveguide, causing reduced transmission to the photodiode. There have been two different approaches to design soft waveguides: encapsulation of the waveguide with a cladding material for total internal reflection [17], [27] and coating of the wall of the waveguide with a reflective layer for internal transmission [25], [26]. Although the cladding method, the same mechanism as that of fiber optics, has an advantage of simple fabrication, it has a design constraint in selection of the cladding material that is required to have a lower refractive index than that of the core. In addition, since the incident angle needs to exceed the critical angle for total internal reflection, at least part of the light always escape from the waveguide even without deformation unless the input light has directionality along the waveguide.

We focus on the method of reflective layer in this study, which has an advantage of reflecting the light in any arbitrary directions emitted from the light source when the waveguide is not deformed. When the waveguide is deformed, microcracks form on the thin reflective metal layer due to its inextensible property compared to the soft elastomer, as shown in Fig. 2. Then, part of the light escapes through the microcracks, resulting in optical power loss that can be easily detected by the photodiode.

Fig. 3 shows the waveguide prototyped in this work. When the waveguide is not deformed, the light propagates to the end. However, with a local contact, the light exits at the contact area

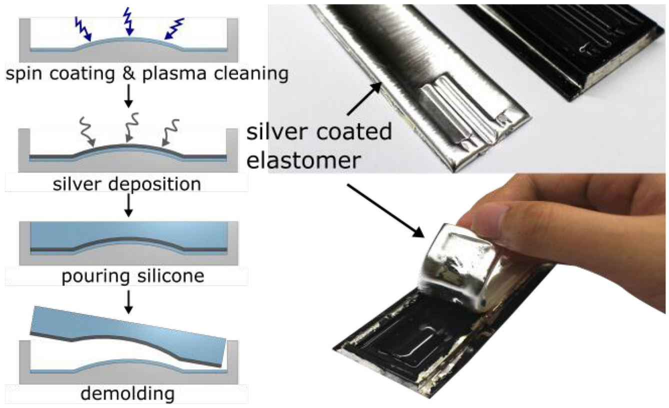

Fig. 4. Schematic of the fabrication process of silver layer(Left), demolding the elastomer with metal layer from the mold (Bottom-Right), Completely fabricated metal layer on the elastomer surface (Top-Right).

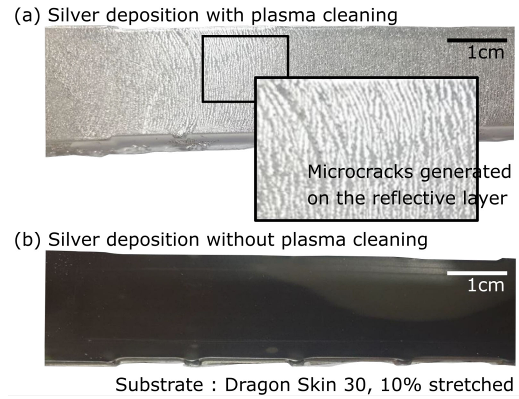

Fig. 5. Result of TVD of silver layer on silicone. Both silicone are stretched up to 10% strain to compare the generation of microcracks. (a) The silicone went under plasma cleaning process. (b) The below one did not went under plasma cleaning process.

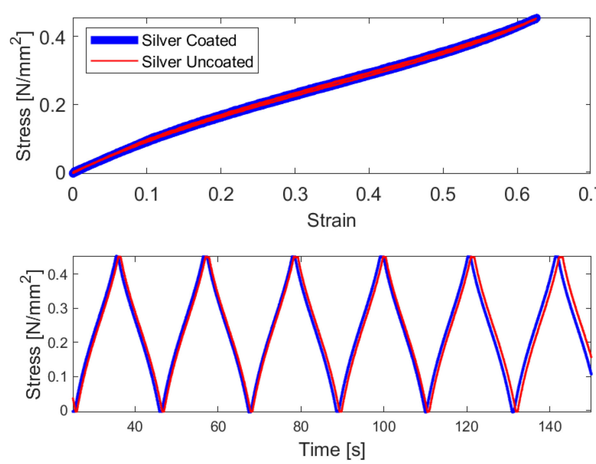

Fig. 6. (a) Stress-Strain Curve of the Dragon Skin 30 with, and without 100 nm of silver layer under 60% of strain. (b) Force-time plot of Dragon Skin 30 with, and without 100 nm of silver layer under 60% of strain.

of the waveguide. This is due to the microcracks formed around the contact area of the waveguide.

The main challenge in this design is fabrication of a uniform and robust reflective metal layer on the surface of a polymer structure mostly made of silicone elastomer. Although metal leafing has been proposed as a simple and low-cost fabrication method [25], it does not guarantee the uniformity and the thickness of the reflective layer due to the heavy involvement of a manual process. As an alternative, a thin film deposition process, such as sputtering or thermal vapor deposition (TVD), has been proposed for better control of thickness and uniformity [26]. However, bonding of a thin metal layer to the polymer substrate was not strong enough to tolerate repeated deformation, so the layer needed to be fully encapsulated by transparent elastomer. In this case, the material for the waveguide is highly limited due to the requirement of transparency. Therefore, we propose a new method of depositing a thin metal layer on a polymer substrate, layer transfer deposition (LTD), in this letter. We were able to not only deposit metal on a highly stretchable material (modulus $<$100 kPa, elongation at break $>$300%) but also achieve strong bonding to the substrate.

B. Layer Transfer Deposition

In the LTD process, we deposit a thin metal layer on a sacrificial polymer layer coated on a mold and then transfer the deposited layer to the host structure, as shown in Fig. 4. We used silver as the material for the reflective layer due to its high optical reflectivity in the range of visible lights and the low cost compared to other metals with high reflectivity, such as gold [28]. The molds were made of ultraviolet (UV)-cured thermoplastic (VeroBlack, Stratasys) using a 3D printer (Objet30, Stratasys), and the body of the sensor-integrated actuator was made of highly stretchable silicone elastomer (Dragon Skin 30, Smooth-On).

First, a thin layer of silicone is prepared on the mold using a spin-coater (SF-150NA, RHABDOS) at 2000 rpm for 30 seconds, and cured in an oven (60 °C, 30 minutes). Then, it is treated with a plasma cleaner (EQ-PCE-3, MTI Corp.) to increase the surface energy for better bonding of silver particles during deposition. It can be seen that the surface treatment process helps bonding of the silver layer to the polymer surface in Fig. 5. With surface treatment (Fig. 5(a)), the silver particles were uniformly deposited to the substrate showing high reflectivity and uniform microcracks. However, without surface treatment (Fig. 5(b)), it is hard to see the silver layer on the substrate even with the same deposition process. After the surface treatment, a 100 nm silver layer is directly deposited on the elastomer surface by TVD, followed by pouring and curing of liquid silicone elastomer on top. When the elastomer is peeled off from the mold after curing, only the metal layer is transferred to the silicone structure with strong adhesion. Since the entire silver layer is transferred from the thin sacrificial layer to the host structure, the coated layer is also highly uniform and reflective.

To ensure that the mechanical property of the polymer is not altered by he reflective layer, 60% of strain was applied to two silicone (Dragon Skin 30, Smooth-On) samples with and without a silver layer multiple times. As shown in the stress-strain curve from the loading-unloading test with multiple loops in Fig. 6, the deposition of the silver layer did not affect the mechanical

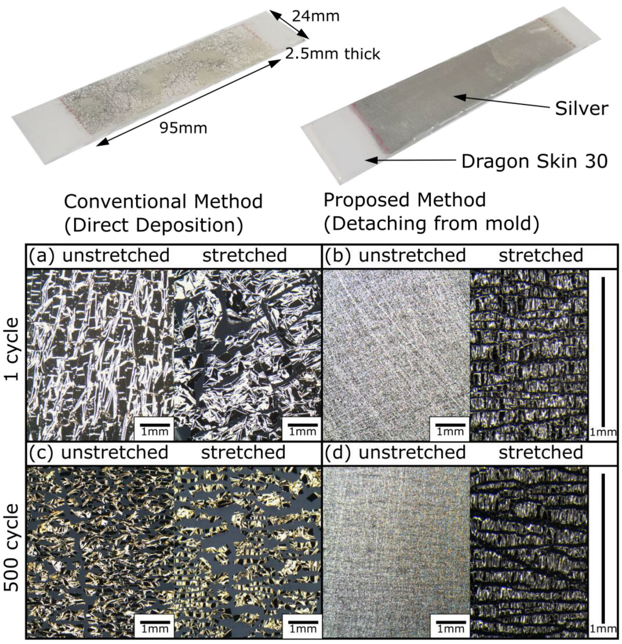

Fig. 7. Result of the cyclic strain test (500 cycles) of silicone specimen with 100 nm of silver layer on its surface. Metal layer of the left specimen was fabricated by direct thermal deposition (Top-Left), while right specimen was fabricated by the proposed method (Top-Right). Top row (a), (b) corresponds to the microscopic view before the cyclic test, and Bottom row (c), (d) is the microscopic view after the cyclic test. Left column (a), (c) corresponds to the metal layer fabricated by direct thermal deposition, and Right column (b), (d) is the layer fabricated by the proposed method.

property of the polymer structure at all. This implies that integration of the sensing structure of an optical waveguide to a soft pneumatic actuator will not change the actuation performance.

C. Metal Layer Robustness Analysis

The robustness of the metal-deposited polymer samples was verified with a cyclic tensile test. In this experiment, cyclic strain up to 50% was applied for 500 cycles to two different specimens made of the same silicone elastomer (length: 95 mm, width: 24 mm, and thickness: 2.5 mm). Fig. 7 compares the quality of the silver layers after initial loading and after loadings of 500 times for direct deposition and LTD. Figs. 7(a) and 7(b) show the microscopic views of the samples before the cyclic test, and Figs. 7(c) and 7(d) show the same samples after the cyclic test. It can be observed that the metal layer made by LTD is almost intact after the cyclic test while that by conventional direct deposition was significantly degraded. This verifies that the metal layer fabricated by the proposed method makes strong adhesion to the elastomer surface. Therefore, we can use the LTD layer inside an air chamber for actuation without covering with another layer of elastomer.

III. Sensor-Integrated Soft Actuator

A. Sensorized Pneumatic Chamber

A soft pneumatic bending actuator has an air chamber, which is inflated or deflated depending on the internal air pressure for bending. Our goal is integration of the optical waveguide into the actuator. By simply coating the inside of the pneumatic air chamber with the reflective layer described in the previous section, the air chamber can be used as a sensing element as well. Since the sensing medium, light, in our sensor has neither mass nor volume, we can make sure that the performance of the actuator will not be affected by addition of the sensor as long as the geometry of the actuator does not change.

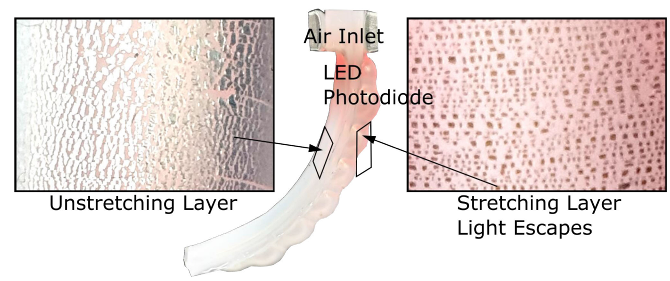

Fig. 8. Prototype of pneumatic actuator with air chamber coated with reflective layer. The right wall of the chamber is thinner than the left one, generating more microcracks. Since light emitted from LED on top is transmitted throughout the chamber, more stretched wall (right) with microcracks shows red light.

The air chamber of the actuator is enclosed by two elastomeric layers, as shown in Fig. 8. Since the two layers are made of different materials with different stiffnesses, only the softer layer stretches, generating bending motions. When the actuator bends, many microcracks formed on the stretched side of the metallic layer, and the light from the LED escapes through the cracks. In Fig. 8, the right portion of the actuator looks more red than the left side, since much more cracks are generated, and a higher density of the light is release from the chamber. The optical power loss measured by the photodiode placed in the chamber can be easily converted to the bending shape of the actuator that is analogous to proprioceptive information in biological actuators (i.e. muscles).

B. Design and Fabrication

Fig. 9 describes the sensor-integrated actuator prototype (a) and the fabrication process. Two elastomeric layers with reflective coatings are produced separately (b-d) and bonded (e). One of the two layers is made of stiff elastomer (Dragon Skin 30, Smooth-On) and does not stretch when the actuator is pressurized. The other layer has multi-material structure made of two materials (Ecoflex 30 and Dragon Skin 30, Smooth-On) placed alternately. When the actuator is pressurized, the softer regions stretch and generate microcracks. The stiffer regions between the soft regions prevent the excessive expansion of the layer in the circumferential direction, amplifying bending motions.

For fabrication, two molds are prepared for the two layers. First, silver layers are deposited on the molds using thermal evaporation (Fig. 9(b)). Then the uncured silicone is poured in the mold (Fig. 9(c)). For the multi-material layer, the prepared cured silicone blocks with a higher stiffnesses are placed in the mold with intervals before the soft silicone is poured. After cured, two cured silicone layers are bonded at the edges together.

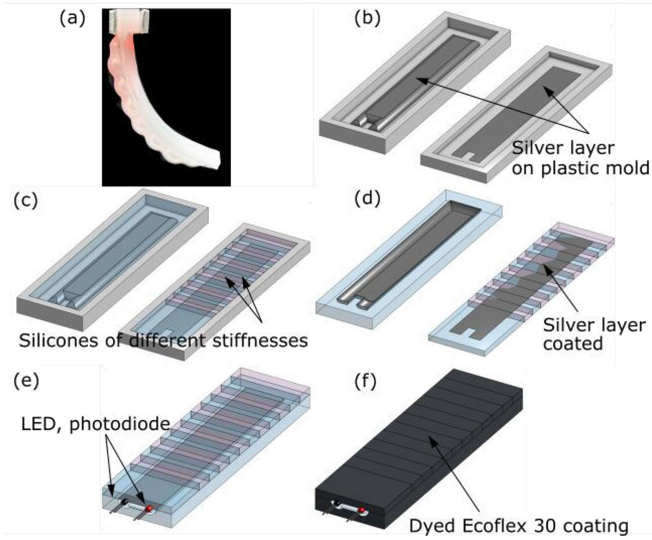

Fig. 9. Fabrication process for the integration of pneumatic actuator and optic sensing. (a) Real prototype of the actuator. (b) Vapor deposition of silver on the spin coated elastomer on the surface of the plastic molds. (c) Pouring two silicone materials to the mold for different stiffnesses for the bending motion. (d) After separation from the mold, silver layers adhere on the molded elastomer. It includes two branches for LED and photodiode for preventing direct transmission of the light. (e) Attaching the two layers and putting LED, photodiode. (f) Coating the whole structure with dyed flexible elastomer for blocking ambient light.

An LED and a photodiode are placed at the same side of the chamber (Figs. 9(d) and 9(e)). They are separated by a partition wall that prevents direct light transmission from the LED to the photodiode. After bonding, pneumatic tubes for actuation are inserted. Finally, the entire structure is coated with a thin layer of elastomer (Ecoflex 30, Smooth-On) dyed with a black pigment (Fig. 9(f)). This outermost black layer blocks ambient lights for reliable sensor readings.

IV. Experiments and Results

A. Experimental Setup

Fig. 10 shows the experimental setup for the characterization of the system. We placed the actuator in the vertical direction as an initial position. For characterizing the dynamics and the sensor signals, we applied pressure inputs through a regulator (SMC, ITV2050), tracked three points on the actuator body, and calculated its curvature from the sensor signals.

B. Characterization

The characterization of the proposed integrated system was defined with input $u \in \mathcal{R}$ (air pressure), state $x \in \mathcal{R}$ (curvature of the actuator), and output $y \in \mathcal{R}$ (sensor signal). Then, the overall system could be modeled by satisfying the following state-space model:

$$\dot{x} = f(x, u) + w$$
$$y = h(x) + v \tag{1}$$

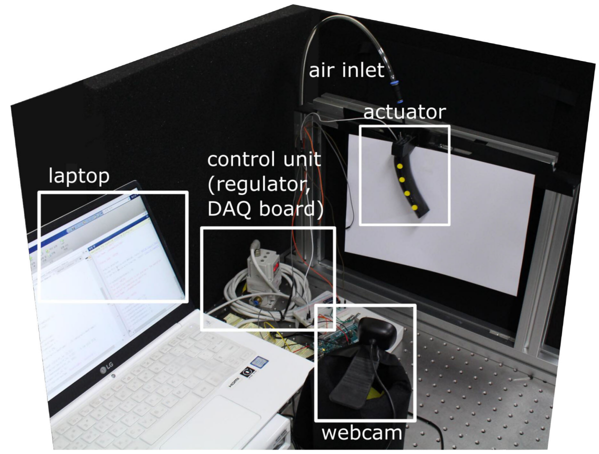

Fig. 10. Experimental setup for characterization of the actuator and sensing. A regulator produces inputs to the system, where the curvature of the system is tracked with a webcam. The sensor signal, output of the system, is measured.

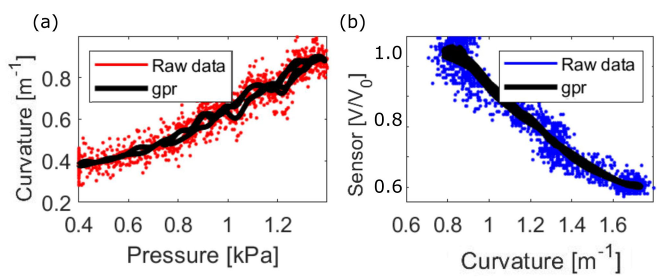

Fig. 11. Characterization of the prototype. (a) Input (pressure)-State (curvature) relation, actuator characterization. (b) State (curvature)-Output (sensor output) relation, Sensor characterization.

where $f : \mathcal{R}^2 \to \mathcal{R}$ and $h : \mathcal{R} \to \mathcal{R}$ are Lipschitz continuous functions, and w, v are the uncertainty and the noise terms. Since we do not have a model for f and h, data-driven function approximation was conducted. In particular, Gaussian process regression (GPR) was used to model the function. GPR is a non-parametric supervised learning technique, which can be formulated as:

$$f \sim \mathcal{GP}(m(x), k(x, x')) \tag{2}$$

where $m(x)$ is a mean function, $k(x, x')$ is a kernel function [29]. Then, the posterior distribution of f given training dataset $\mathcal{D}$ can be written as $f \mid \mathcal{D} \sim \mathcal{N}(\mu, \Sigma)$ where each components are defined as:

$$\begin{aligned} \mu &= k(X, x)^T k(X, X)^{-1} y \\ \Sigma &= k(x, x') - k(X, x)^T k(X, X)^{-1} k(X, x') \end{aligned} \tag{3}$$

where X and y are inputs and outputs of the training dataset, respectively. Training datasets were gathered by inserting a custom input sequence of different frequencies to the system and collecting the state and the output. Fig. 11 shows the result of the characterization. The curvature of the system changed non-linearly to the input pressure as general pneumatic systems

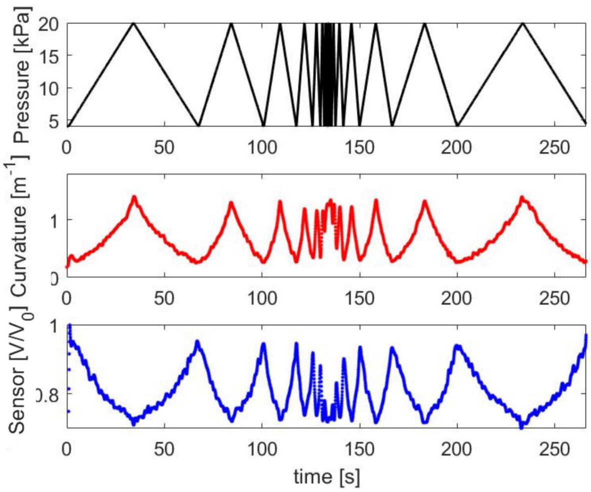

Fig. 12. Dynamic response of the actuator and sensor with various frequencies of inputs. Sign of the sensor data was inverted for better interpretation. Due to regulating limit and inherent property of the material, actuator dynamics showed upper limit on the dynamic bandwidth. However the sensor dynamics was sufficiently fast to track the bending of the actuator.

does. Little hysteresis was observed in the result which came from the viscoelasticity of the actuator material. The sensor produced linear signals to the curvature. The sensor voltage dropped as the curvature increased, due to the loss of the light through microcracks. The noise level of the sensor data was measured under constant pressure input (20 kPa). The standard deviation of the sensor data during 15 seconds of a time interval was 0.025 $[V/V_0]$. The voltage difference of 0.025 $[V/V_0]$ is equivalent to the curvature difference of 0.14 mm^{-1}, and the pressure difference of 0.17 kPa from the characterization result in Fig. 11.

Fig. 12 shows the response of the system to the input pressure frequencies of 0.015, 0.03, 0.06, 0.125, 0.25, 0.5, 1, 2, and 5 Hz to analyze the dynamic properties of the system. Due to the slow and discrete air regulation and the inherent slow response of the pneumatic actuation system, the actuator dynamics expressed in red was not able to follow the inputs with high frequencies, but followed well up to 1 Hz. Compared to that, the sensor signal expressed in blue showed a fast response to the curvature input. In Fig. 12, since the working frequency of our system of interest is less than 5 Hz, the sensor data was filtered with a low-pass filter (LPF) with a cut-off frequency of 5 Hz.

The states were post-calibrated referring the vision tracking camera data. A kernel function was a squared-exponential function, and Quasi-Newton convex optimization was used to determine hyperparameters of the kernel function.

C. System Robustness

Thanks to the robustness of the proposed LTD method, the sensor integrated actuator worked robustly over repeated uses while experiencing minimum performance degradation. Fig. 13 is the result of a cyclic test of 850 cycles with minimum 4 kPa and maximum 20 kPa pressure inputs. The sensor signal showed a transient period before it was stabilized after 500 cycles.

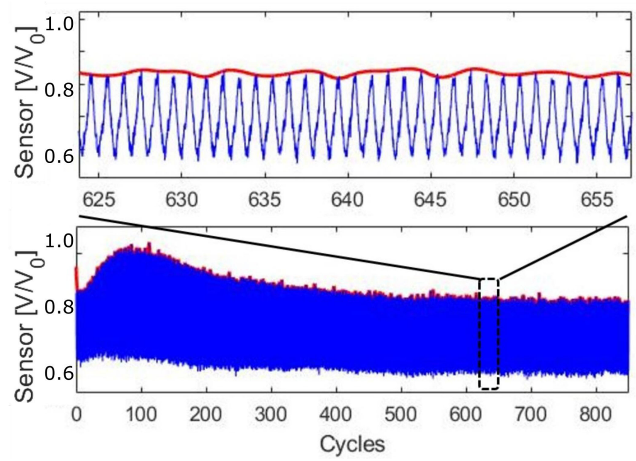

Fig. 13. Result of cyclic test of the prototype. 850 cycles of pressurization (20 kPa) and depressurization (4 kPa) of the prototype were done.

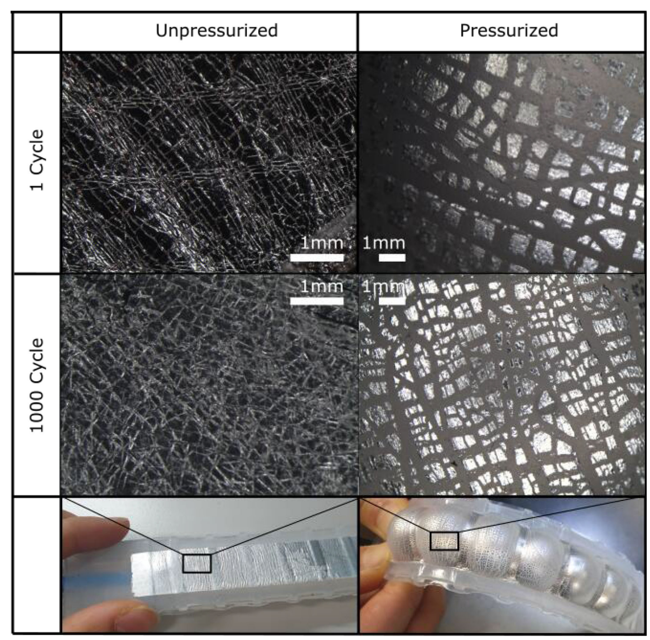

Fig. 14. Microscopic view of silver layer before (Top row), and after (Middle row) cyclic pressurizing test (12.5 kPa, 1000 cycles).

The transient region is first due to the property of the silicone material, which needs a training period. Meanwhile, it is required that the sensor signal itself has minimal transition. Fig. 14 shows the metal layer and the generation of microcracks in pressurized and unpressurized states before and after the cyclic test. As expected from the tensile cyclic test in Fig. 7, the layer showed little degradation.

D. Control Strategy and Results

The proposed system calibration model of Equation (1) may be imperfect due to several issues, such as hysteresis, noises, and modeling errors. Also, to control the system to track the reference state, we need an optimal state observer to the system,

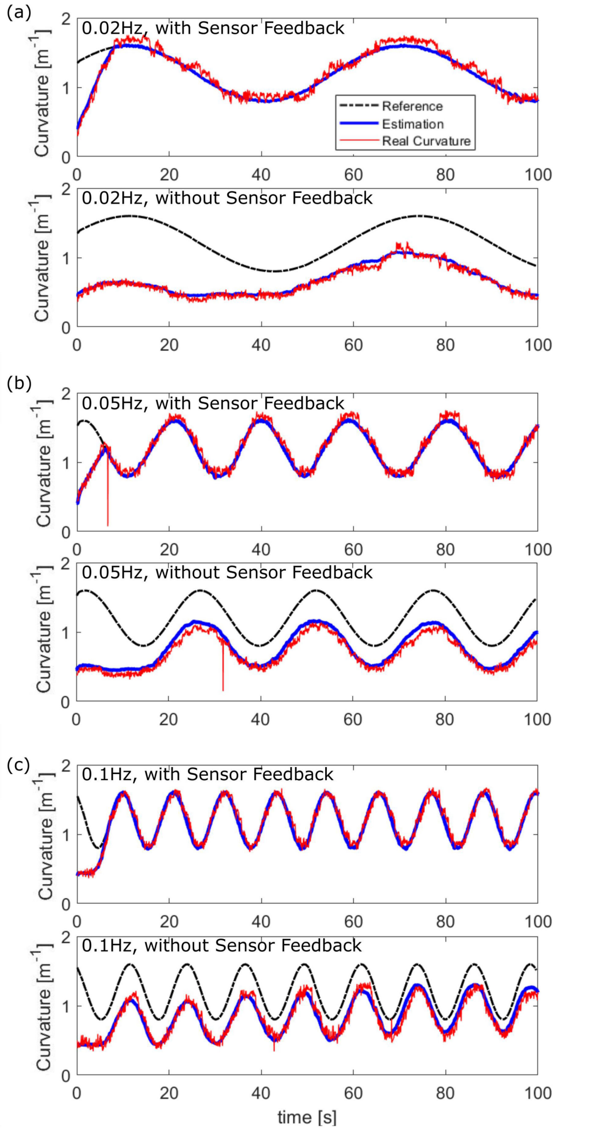

Fig. 15. Reference tracking control experiment of the prototype with (Top) and without (Bottom) sensor feedback. Various frequency of reference curvature were tracked; (a) 0.02 Hz, (b) 0.05 Hz, (c) 0.1 Hz.

and we used extended Kalman filter (EKF) as a state estimator [30]. Further, in order to consider the modeling uncertainty while controlling the system, we adopt sliding mode control (SMC) to control the system to track the desired curvature.

First, we convert the system Equation (1) to control-affine form by performing time derivative of the system:

$$\ddot{x} = \frac{\partial f}{\partial x}\dot{x} + \frac{\partial f}{\partial u}\dot{u} = \frac{\partial f}{\partial x}(f(x,u)+\delta) + \frac{\partial f}{\partial u}\dot{u} \quad (4)$$

where δ is the uncertainty term of the system equation $f(x,u)$, in which its norm is bounded by k. Then, we introduce a sliding variable $s = \dot{x} + \lambda x$ to obtain a stabilizing feedback control law:

$$\dot{u} = \frac{1}{F_u}\{-k\,\mathrm{sgn}(\dot{x}+\lambda x) - F_x f(x,u) - \lambda\dot{x}\} \quad (5)$$

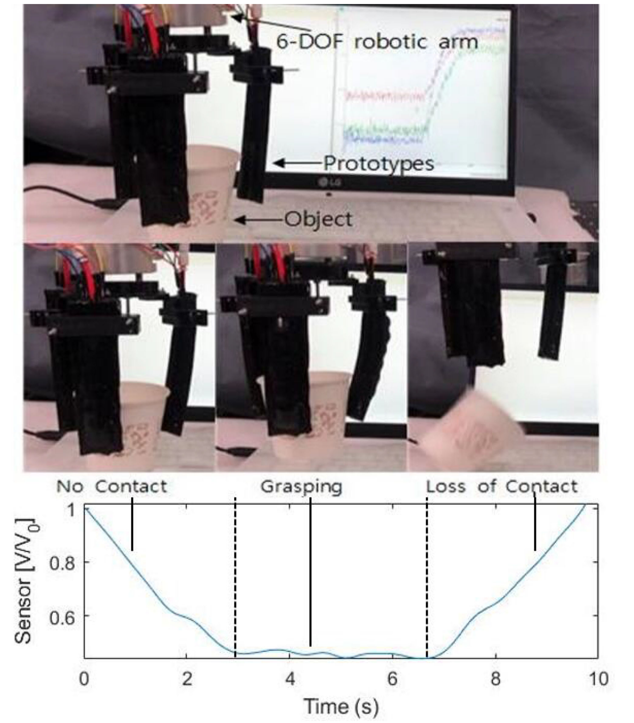

Fig. 16. Application experimental setup (Top) and results of the sensor signal of the gripper (Bottom).

where $F_x = \frac{\partial f}{\partial x}$ and $F_u = \frac{\partial f}{\partial u}$. To track the reference $x \rightarrow x_d$, terms $\dot{x}$ and x should be changed to the error dynamics (i.e., $e = x - x_d$).

Fig. 15 shows the result of the tracking control of the reference curvature, which was given as a sinusoidal function with respect to time, with different frequencies. The upper plots show the result of the closed-loop control with sensor feedback, while the lower plots show the result of the open-loop control without feedback. The result of the open-loop control showed that the error did not converge to zero, while the closed-loop control showed considerable improvements by the integration of the sensor.

V. Application

Three prototypes were attached on the end effector of a commercial six degrees-of-freedom (DOF) robotic arm (UR3, Universal Robots) to demonstrate the application of our actuator as a soft robotic gripper. When the actuator bends to grasp an object, each actuator shows a signal drop of the sensor output. While holding the object, the sensor output stays in the same level. When the actuator releases the object, the output signal goes back to the original level, as shown in Fig. 16.

VI. Discussion and Future Work

In this letter, a concept of the integration of a pneumatic bending actuation and an its proprioceptive sensing by optical waveguide was suggested, with which a common problem of estimating the state of a soft robotic system could be resolved. We especially focused on the pneumatic bending actuator, which has raised a main challenge due to the difficulty of integration in the sense of the structural constraints. This problem was solved by the proposed concept, which was embodied by integrating the air chamber of a pneumatic actuator and an optical waveguide of a sensor. To optically sensorize the air chamber, we coated its wall with a reflective metal layer using layer transfer deposition. This fabrication method enabled deposition of a uniform metal layer on a polymer substrate with strong adhesion, increasing the durability and the reliability of the sensor. A prototype of the sensor-integrated soft actuator was fabricated to test the performance of the sensor. The characterization result demonstrated a potential in controlling soft actuator systems. The soft robotic gripper was proposed as an application, capable of sensing the curvature of the gripper and further estimating the size of the gripping object.

While the sensor data shows the curvature of the actuator caused by pressure input, the actuator can deform to a more complex geometry due to the external force, or displacement. We plan to improve the sensing structure by modifying the geometry or integrating additional sensor on the surface of the prototype to distinguish deformation caused by internal actuation pressure from external disturbances. We also aim to utilize infrared light instead of visible light to isolate our sensing system from the interference of ambient lights.

VII. Conclusion

Integration of the air chamber of a pneumatic actuator and an optical waveguide of a sensor was proposed. To optically sensorize the air chamber, we coated its wall with a reflective metal layer using our fabrication method called layer transfer deposition. This fabrication method enabled deposition of a uniform metal layer on a polymer substrate with strong adhesion, increasing the durability and the reliability of the sensor. A prototype of sensor-integrated soft actuator was fabricated to test the performance of the sensor. The result of characterization of the prototype demonstrated a potential in controlling soft actuator systems. The soft robotic gripper was proposed as an real world application.

References

[1] M. A. Goodrich *et al.*, “Human–robot interaction: A survey,” *Found. Trends Hum. Comput. Interact.*, vol. 1, no. 3, pp. 203–275, 2008.

[2] S. G. Khan, G. Herrmann, M. Al Grafi, T. Pipe, and C. Melhuish, “Compliance control and human–robot interaction: Part 1—survey,” *Int. J. Hum. Robot.*, vol. 11, no. 3, 2014, Art. no. 1430001.

[3] S. Kim, C. Laschi, and B. Trimmer, “Soft robotics: A bioinspired evolution in robotics,” *Trends Biotechnol.*, vol. 31, no. 5, pp. 287–294, 2013.

[4] C. Majidi, “Soft robotics: A perspective—current trends and prospects for the future,” *Soft Robot.*, vol. 1, no. 1, pp. 5–11, 2014.

[5] B. Mosadegh *et al.*, “Pneumatic networks for soft robotics that actuate rapidly,” *Adv. Funct. Mater.*, vol. 24, no. 15, pp. 2163–2170, 2014.

[6] K. C. Galloway, P. Polygerinos, C. J. Walsh, and R. J. Wood, “Mechanically programmable bend radius for fiber-reinforced soft actuators,” in *Proc. IEEE Int. Conf. Adv. Robot.*, 2013, pp. 1–6.

[7] C.-P. Chou and B. Hannaford, “Measurement and modeling of mckibben pneumatic artificial muscles,” *IEEE Trans. Robot. Autom.*, vol. 12, no. 1, pp. 90–102, Feb. 1996.

[8] R. Ozawa, K. Hashirii, and H. Kobayashi, “Design and control of underactuated tendon-driven mechanisms,” in *Proc. IEEE Int. Conf. Robot. Autom.*, 2009, pp. 1522–1527.

[9] H. In, B. B. Kang, M. Sin, and K.-J. Cho, “Exo-glove: A wearable robot for the hand with a soft tendon routing system,” *IEEE Robot. Autom. Mag.*, vol. 22, no. 1, pp. 97–105, Mar. 2015.

[10] S. Seok, C. D. Onal, K.-J. Cho, R. J. Wood, D. Rus, and S. Kim, “Meshworm: a peristaltic soft robot with antagonistic nickel titanium coil actuators,” *IEEE/ASME Trans. Mechatron.*, vol. 18, no. 5, pp. 1485–1497, Oct. 2012.

[11] H. Jin, E. Dong, M. Xu, C. Liu, G. Alici, and Y. Jie, “Soft and smart modular structures actuated by shape memory alloy (sma) wires as tentacles of soft robots,” *Smart Mater. Struct.*, vol. 25, no. 8, 2016, Art. no. 085026.

[12] Y. Bar-Cohen and Q. Zhang, “Electroactive polymer actuators and sensors,” *MRS Bull.*, vol. 33, no. 3, pp. 173–181, 2008.

[13] M. Ortiz, F. Shelton IV, and J. Swayze, “Electroactive polymer-based articulation mechanism for grasper,” Jan. 4 2011, US Patent 7,862,579.

[14] F. Connolly, C. J. Walsh, and K. Bertoldi, “Automatic design of fiber-reinforced soft actuators for trajectory matching,” *PNAS*, vol. 114, no. 1, pp. 51–56, 2017.

[15] R. F. Shepherd *et al.*, “Multigait soft robot,” *PNAS*, vol. 108, no. 51, pp. 20 400–20 403, 2011.

[16] T. Giffney *et al.*, “Soft pneumatic bending actuator with integrated carbon nanotube displacement sensor,” *Robotics*, vol. 5, no. 1, 2016, Art. no. 7.

[17] H. Zhao, K. O’Brien, S. Li, and R. F. Shepherd, “Optoelectronically innervated soft prosthetic hand via stretchable optical waveguides,” *Sci. Robot.*, vol. 1, no. 1, 2016, Art. no. eaai7529.

[18] R. A. Bilodeau, E. L. White, and R. K. Kramer, “Monolithic fabrication of sensors and actuators in a soft robotic gripper,” in *Proc. IEEE/RSJ Int. Conf. Intell. Robot. Syst.*, 2015, pp. 2324–2329.

[19] Y.-L. Park, B.-R. Chen, and R. J. Wood, “Design and fabrication of soft artificial skin using embedded microchannels and liquid conductors,” *IEEE Sens. J.*, vol. 12, no. 8, pp. 2711–2718, Aug. 2012.

[20] J.-B. Chossat, H.-S. Shin, Y.-L. Park, and V. Duchaine, “Soft tactile skin using an embedded ionic liquid and tomographic imaging,” *J. Mech. Robot.*, vol. 7, no. 2, 2015, Art. no. 021008.

[21] S. Choi and Z. Jiang, “A novel wearable sensor device with conductive fabric and pvdf film for monitoring cardiorespiratory signals,” *Sens. Actuaors, A*, vol. 128, no. 2, pp. 317–326, 2006.

[22] T. Kim, J. Park, S. J. Yoon, D. H. Kong, H.-W. Park, and Y.-L. Park, “Design of a lightweight inflatable sensing sleeve for increased adaptability and safety of legged robots,” in *Proc. IEEE Int. Conf. Soft Robot. (RoboSoft)*, 2019, pp. 257–264.

[23] S. C. Mannsfeld *et al.*, “Highly sensitive flexible pressure sensors with microstructured rubber dielectric layers,” *Nature Mater.*, vol. 9, no. 10, 2010, Art. no. 859.

[24] A. Frutiger *et al.*, “Capacitive soft strain sensors via multicore–shell fiber printing,” *Adv. Mater.*, vol. 27, no. 15, pp. 2440–2446, 2015.

[25] C. To, T. L. Hellebrekers, and Y.-L. Park, “Highly stretchable optical sensors for pressure, strain, and curvature measurement,” in *Proc. IEEE/RSJ Int. Conf. Intell. Robot. Syst.*, 2015, pp. 5898–5903.

[26] C. To, T. Hellebrekers, J. Jung, S. J. Yoon, and Y.-L. Park, “A soft optical waveguide coupled with fiber optics for dynamic pressure and strain sensing,” *IEEE Robot. Autom. Lett.*, vol. 3, no. 4, pp. 3821–3827, Oct. 2018.

[27] C. K. Harnett, H. Zhao, and R. F. Shepherd, “Stretchable optical fibers: Threads for strain-sensitive textiles,” *Adv. Mater. Technol.*, vol. 2, no. 9, 2017, Art. no. 1700087.

[28] H. W. Edwards and R. P. Petersen, “Reflectivity of evaporated silver films,” *Phys. Rev.*, vol. 50, no. 9, 1936, Art. no. 871.

[29] C. E. Rasmussen and Z. Ghahramani, “Bayesian monte carlo,” in *Proc. Adv. Neural Inf. Process. Syst.*, 2003, pp. 505–512.

[30] H. K. Khalil, *Nonlinear Systems*, 3rd ed. Upper Saddle River, NJ, USA: Prentice-Hall, 2002.